Arch. Metall. Mater. **66** (2021), 1, 5-14

DOI: 10.24425/amm.2021.134752

D. MIGAS[1*], M. KIERAT[1], G. MOSKAL[1]

THE OXIDE SCALES FORMED ON DIFFERENT Co-Ni BASED SUPERALLOYS DURING ISOTHERMAL OXIDATION AT 800 AND 900°C

In this investigation, the formation of oxide scales on different Co-Ni based superalloys of γ–γ' type was analyzed. Co-20Ni-7Al-7W (at. %) alloy as well as its W-free modifications based on Co-Ni-Al-Mo-Nb and Co-Ni-Al-Ta systems was analyzed under conditions of high temperature oxidation at 800 and 900°C. Therefore, the alloys were isothermally oxidized at selected temperatures for 100 h in laboratory furnace. Afterwards, the oxidation products were evaluated by means of X-ray diffraction (XRD), optical microscopy (OM) and scanning electron microscopy (SEM). The performed tests showed that W-free alloys exhibit worse oxidation resistance compared to those of Co-Ni-Al-W alloys. After oxidation at 900°C, all alloys were prone of oxide spallation. The scales characterized by oxide peeling were mostly composed of complex Co-based oxides, including $CoWO_4$, $CoTa_2O_6$, $Co_2Mo_3O_8$, $CoNb_2O_6$.

Keywords: γ–γ' cobalt-based superalloys, high temperature oxidation, Co-Ni superalloy, W-free cobalt superalloys

1. Introduction

Co-based superalloys of γ–γ' type are a new class of high temperature materials suitable for operating at high temperature under detrimental conditions. Although alloys are in the basic research phase, their potential area of application is connected with power generation and aircraft industries. The promising properties of new alloys such as high melting point, excellent creep and fatigue resistance allow to consider these materials for application in highly loaded high temperature components, mainly in parts of gas turbines. The landmark work concerning these materials was published in 2006 [1]. The publication showed presence of γ'-Co_3(Al, W) phase in ternary Co-Al-W system. Since this time, the article achieved over 500 citations. The basic trend in development of Co-based superalloys is tailoring of chemical composition in order to improve phase stability and *solvus* temperature of γ' phase as well as to decrease density of alloys. Therefore, numerous investigations were performed in order to evaluate other γ'-forming systems such as Co-Al-V [2], Co-Al-Mo-Nb [3], Co-Ta-V [4], Co-V-Ti [5] and other. In the case of novel Co-based alloys, substantial amount of Ni is added in order to improve solvus temperature of γ' phase [6].

This article concerns another aspect of superalloys' properties, namely, resistance of alloys to high temperature oxidation. Numerous papers regarding oxidation behavior of alloys based on Co-Al-W system were published. In the case of these alloys, the external scale is composed of simple oxides such as CoO and Co_3O_4; these oxides grow on a top of alloy surface. Underneath, inner oxide layer being mixture of different oxides (mainly $CoWO_4$) is formed as a result of internal oxidation. Beneath this zone, Al-depletion leads to formation of a detrimental phase with formula Co_3W, which is characterized by needle-like morphology. Although many articles concerning high temperature oxidation of alloys based on ternary Co-Al-W system are available, the literature data is poorer in information regarding oxidation of Co-Ni based alloys. H.-Y. Yan et al. investigated the influence of different alloying elements (including Ni) on high temperature oxidation od Co-Al-W based alloys [7-11]. Weiser et al. investigated the influence of Co to Ni ratio in γ'-strengthened alloys on oxidation resistance and the halogen effect at 900°C [12], whereas B. Gao described high temperature oxidation behavior of Co-based superalloys with different Ni content [13]. Furthermore, S. M. Das published article concerning oxidation of W-free Co-Ni-Al-Mo-Ta superalloy [14]. The articles concerning oxidation properties of W-free alloys

[1] SILESIAN UNIVERSITY OF TECHNOLOGY, FACULTY OF MATERIALS ENGINEERING, DEPARTMENT OF ADVANCED MATERIALS AND TECHNOLOGIES, 8 KRASIŃSKIEGO STR., 40-019 KATOWICE, POLAND

* Corresponding author: damian.migas@polsl.pl

based on Co-Al-Mo-Nb system were published by authors of work [15,16].

In the present paper, oxidation behavior of other Co-Ni based alloys was examined. The characterization of the oxidation performance of alloys included microstructural analysis of oxidation products formed on different Co-Ni superalloys. The investigated alloys were based on Co-Ni-Al-Mo-Nb and Co-Ni-Al-Ta systems. The oxidation performance of W-free alloys was compared to that of Co-20Ni-7Al-7W (at. %) alloy.

2. Materials and methods

The Co-20Ni-7Al-7W, Co-20Ni-10Al-5Mo-2Nb and Co-20Ni-7Al-7Ta (at.%) alloys were prepared via vacuum induction melting. The ø20 mm ingots were melted using furnace VSG 02 Balzers and casted under Ar atmosphere. Pure Co, Ni, Al, W, Mo, Nb, Ta metals were used in a preparation of the investigated materials. The alloys were melted in the temperature range 1600÷1700°C in a time of approx. 10 min. The investigated alloys were casted into graphite molds, under the Ar protective atmosphere. The alloys were characterized by dendritic microstructure, typical for casting with high cooling rate. For cobalt alloys where W was replaced by Mo and Nb, occurrence of some eutectic phases in interdendritic regions was observed. In the case of Ta-containing alloy, numerous Ta-rich phases were observed in the as-cast state. The primary microstructure of Co-20Ni-7Al-7W and Co-20Ni-10Al-5Mo-2Nb was described in other works [17,18]

The alloys were investigated in as-cast state. After casting, metal slices of 3 mm thickness were cut from the casted ingot, and then, each piece was cut in half. Surfaces of prepared metal specimens were ground, cleaned and degreased. The samples were exposed to isothermal oxidation at 800 and 900°C for 100 hours. The oxidation tests were carried out in a laboratory furnace working in air. The test temperatures were selected basing on TG analysis and potential operating temperatures of superalloys. The oxidation time of 100 h, sufficient to observe phenomena in oxidized scale, was selected based on experimental experience.

The characterization of oxidation products included investigation of phase composition and analysis of microstructure in cross section of a specimen. The phase composition of upper part of the scale was analyzed by X-ray diffraction (XRD). The cross-sectional analysis of a microstructure was performed by means of light microscopy (LM) and scanning electron microscopy (SEM). The LM micrographs were performed using the Nikon Eclipse MA200 microscope. The specimens were not etched. In the case of SEM/EDS analysis, the scanning electron microscope (SEM, Hitachi S-3400N) equipped with the energy dispersion spectrometer (EDS, Thermo Noran System Seven) was used. The X-ray diffraction measurements in Bragg-Brentano geometry were done using Phillips X'Pert^3 Powder diffractometer fitted with a copper anode tube ($\lambda_{CuK\alpha}$ – 1.54178 Å), operating at 30 mA/40 kV. Recording was performed with a stepwise approach of 0.02° step in the range of 10 to 90° 2θ. Furthermore, thermogravimetric analysis of as-cast alloys under non-isothermal conditions was performed on NETZSCH STA 449 F3 Jupiter device from 40 to 1200°C. The specimens ~4×4×10 mm used in the investigation were ground using SiC paper down to 1200 grid and ultrasonically cleaned in acetone. The oxidation of samples contained in Al_2O_3 crucibles was carried out in air at heating rate 5°C min^{-1}.

3. Results and discussion

The results of thermogravimetric analysis under non-isothermal conditions are shown in Fig. 1. The increase of mass shown by TG plots imply that W-free alloys could be characterized by similar of even faster rate of oxidation at high temperatures compared to that of Co-20Ni-7Al-7W (at. %) alloy. Moreover, the obtained curves were compared to that of basic Co-9Al-9W (at. %) alloy, which was characterized by even lower oxidation rate. However, this alloy contains more Al and W compared to that of Co-Ni-Al-W alloy, which is reason of better oxidation resistance [10]. The highest mass gain was observed for Co20Ni-7Al-7Ta (at. %) alloy. The oxidation rate of all alloys was substantially increased above 900°C.

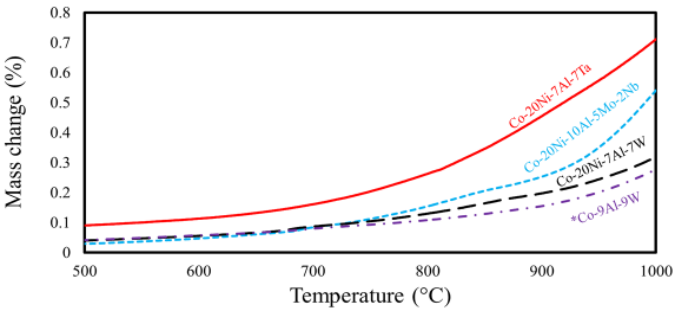

Fig. 1. TG curves of investigated Co-Ni superalloys

Fig. 2. shows macrographs of all investigated specimens after high temperature oxidation at 800 and 900°C. After high temperature exposure at 800°C, a relatively uniform external oxide layer may be observed for Co-20Ni-7Al-7W and Co-20Ni-7Al-7Ta (at. %) alloys. In the case of Co-20-Ni-10Al-5Mo-2Nb (at. %) alloy, oxidation products of different color were observed, this is connected with spallation of an external layer of Co-oxides. Such appearance of oxidized specimens is observable for all alloys oxidized at 900°C. At higher temperatures, the substantial spallation of oxide layer occurred in the case of all Co-Ni based superalloys, and is connected with a generation of stress in the oxide scale during cooling to room temperature.

The phases detected in the scale after isothermal oxidation of Co-20Ni-7Al-7W (at. %) alloy at 800 and 900°C may be seen in Fig. 3. In the case of oxidation at 800°C (Fig. 3a), the recognized phases are single Co-based oxides such as Co_3O_4 and CoO. These oxidation products are related with the external layer of scale formed on Co alloys as a result of external oxidation [9]. The dominant oxide is Co_3O_4,which is thermodynamically

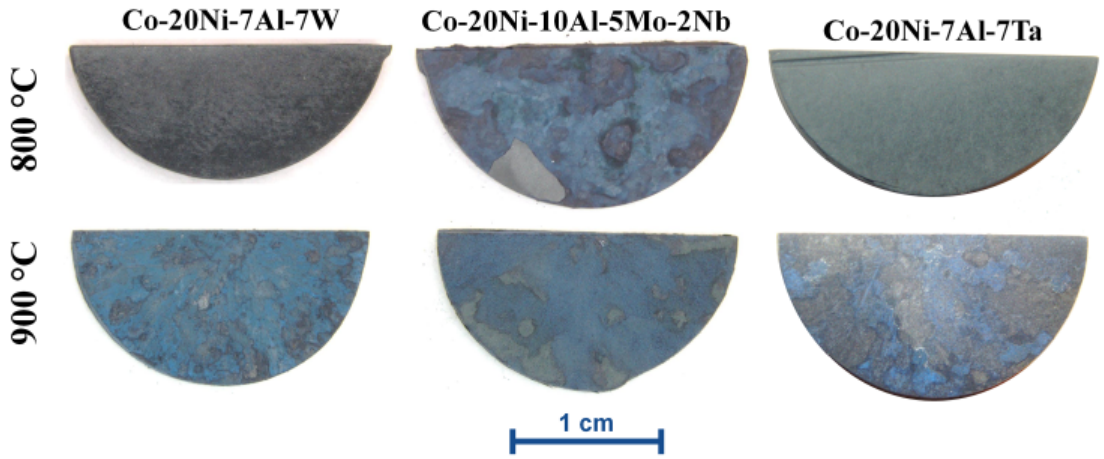

Fig. 2. Macrographs of specimens after oxidation at 800 and 900°C

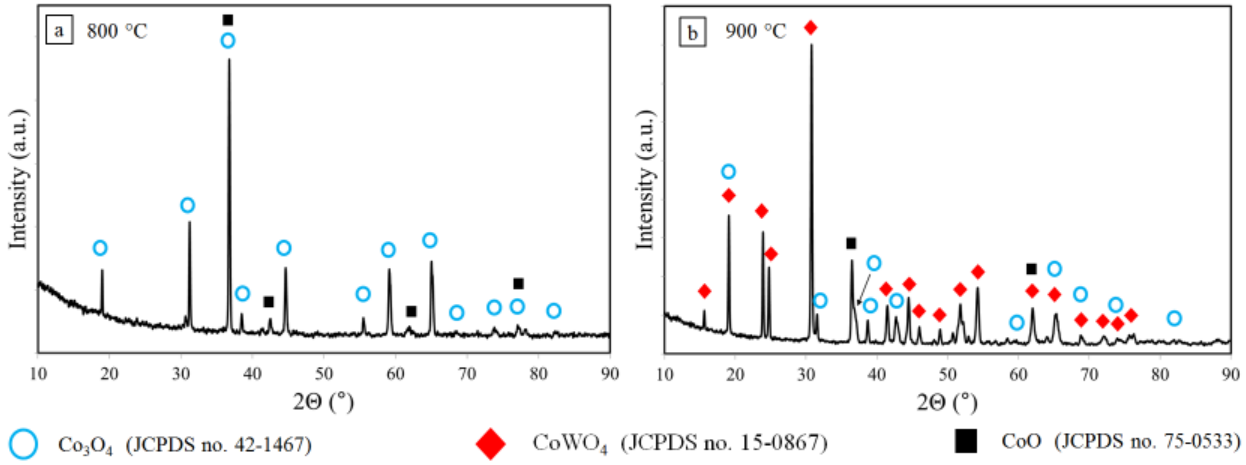

Fig. 3. X-ray diffraction patterns of Co-20Ni-7Al-7W after oxidation at: a) 800°C; b) 900°C

preferred to grow on the top of the scale [19]. After long-term oxidation of Co-Ni-Al-W alloy at 900°C, the dominant recognized oxide was $CoWO_4$ (Fig. 3b). Such type of oxide is normally a component of oxide mixture in an inner oxide layer in the case of oxidation of new Co-based superalloys. Co_3O_4 and CoO oxides were also detected. The peaks corresponding to Co_3O_4 may also be related with presence of $CoAl_2O_4$ (JCPDS no. 44-0160) due to quite similar XRD data. Such phase composition is in accordance with observed spallation of the external layer (Fig. 2).

Fig. 4 shows phases detected in the oxidized surface of Co-20Ni-10Al-5Mo-2Nb (at. %) alloy after oxidation tests at 800 and 900°C. At both temperatures, similar phase constituents were

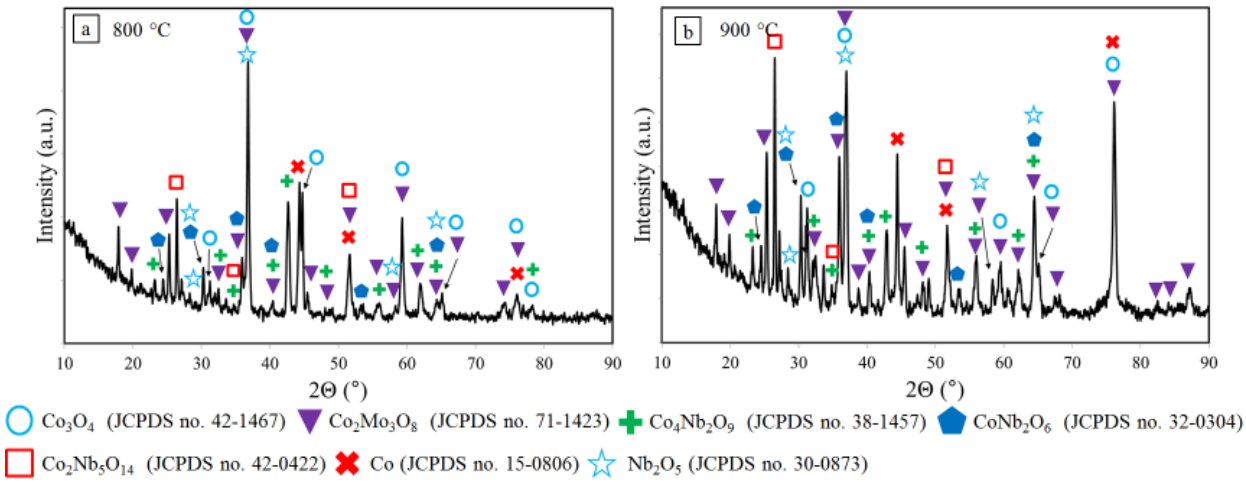

Fig. 4. X-ray diffraction patterns of Co-20Ni-10Al-5Mo-2Nb after oxidation at: a) 800°C; b) 900°C

recognized. The scale structure contains mixture of numerous complex oxides, including $Co_2Mo_3O_8$, $CoNb_2O_6$, $Co_4Nb_2O_9$, and $Co_2Nb_5O_{14}$. Moreover, simple oxides Co_3O_4 and Nb_2O_5 were detected. Similarly to the case of previous alloy, the presence of $CoAl_2O_4$ may not be excluded. Except of oxides, peaks corresponding to solid solution of Co were recognized.

In the case of oxidation products grown on Co-20Ni-7Al-7Ta (at. %) alloy at 800°C (Fig. 5a), only Co_3O_4 oxide was recognized. It is connected with the fact that the external layer of Co-oxide did not spall after cooling to room temperature, similarly to that of Co-20Ni-7Al-7W (at. %) alloy. In this case, phases from inner oxide layer were not detected. Fig. 5b shows a phase

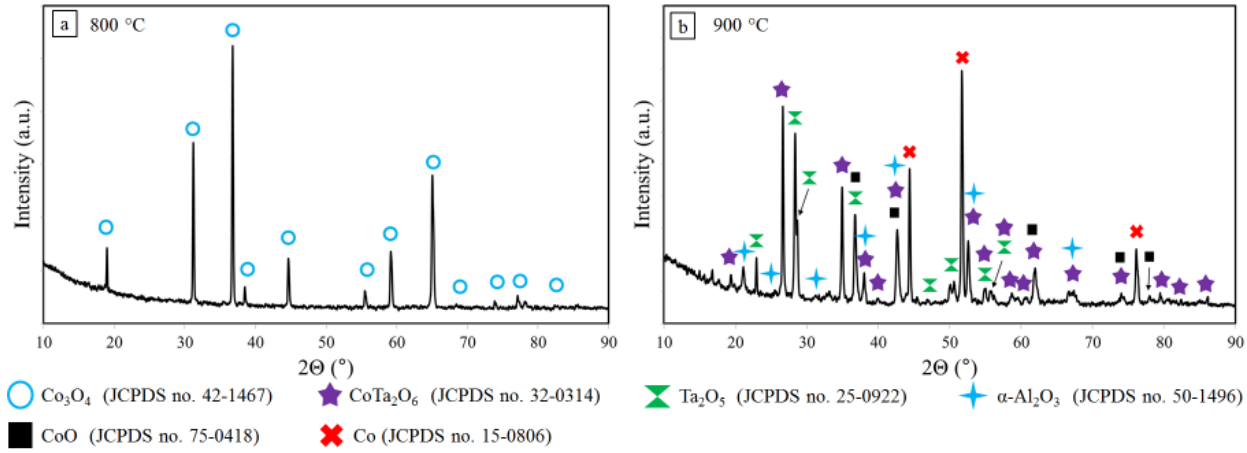

Fig. 5. X-ray diffraction patterns of Co-20Ni-7Al-7Ta after oxidation at: a) 800°C; b) 900°C

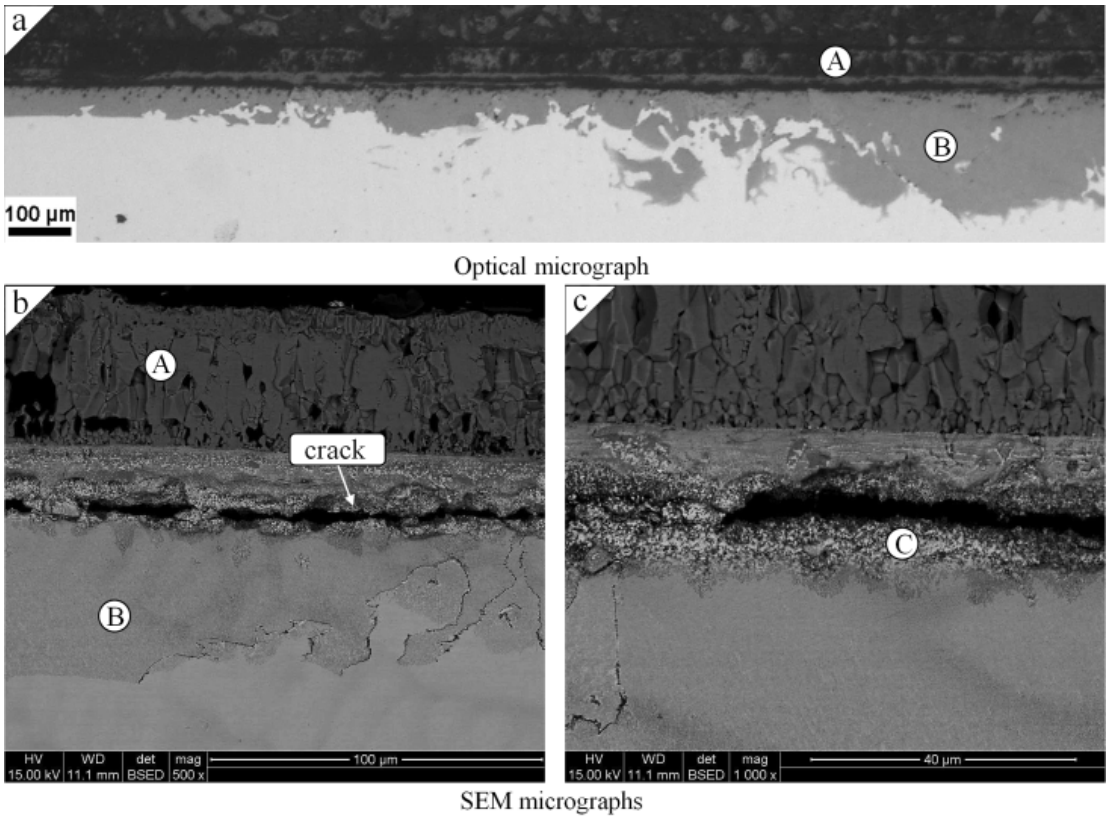

d

Micro-area chemical composition in zones marked in SEM micrographs

Element/Area	Atomic%					Weight%				
	O	Al	Co	Ni	W	O	Al	Co	Ni	W
A	+	-	100	-	-	+	-	100	-	-
B	+	12.3	39	35.8	12.9	+	4.7	32.4	29.6	33.3
C	+	15.5	50.3	9.3	24.9	+	4.9	34.8	6.4	53.9

Fig. 6. Cross-sectional micrographs of the scale grown on Co-20Ni-7Al-7W alloy after oxidation at 800°C: a) LM micrograph; b and c) SEM micrographs; d) EDS analysis

structure of the scale after oxidation at 900°C. After cooling from this temperature, the external layer mostly peeled, therefore, the inner oxide zone was uncovered. In this zone, the dominant oxide phases were $CoTa_2O_6$ and Ta_2O_5. Moreover, some peaks corresponding to α-Al_2O_3 may be observed. The X-ray diffraction pattern showed substantial content of cobalt that suggest the amount of oxides that remain unspalled was very low.

The next part of investigation concerend analysis of the cross-sectional microstructure of oxides grown during high temperature exposure. Fig. 6a shows LM micrograph of the scale grown on the Co-20Ni-7Al-7W (at. %) substrate at 800°C. At least two characteristic areas may be observed. The first one (marked by letter "A") is the external, porous layer of single Co-based oxides which were detected via XRD analysis. This zone is characterized by thickness of c a. 40 µm. The second area (marked by letter "B") is an inner oxide layer. The right side of micrograph reveals that in some parts, the internal oxidation was intensive, and the thickness of inner oxide layer was c. a. 200 µm. SEM micrographs (Fig. 6b and Fig. 6c) show occurrence of the previously mentioned zones. Moreover, a thin area characterized by brighter contrast may be noticed (marked by letter "C"). Such BSE image contrast imply enrichment in elements with high atomic numer, i. e. in tungsten. The previously mentioned area may be composed in a great extent of $CoWO_4$ oxide, which is often met complex oxide in the inner oxide layer in the case of cobalt alloys. Moreover, this phase was recognized via X-ray diffraction after oxidation at higher temperature. Except of W, the analysis of chemical composition in micro areas showed occurrence of Co, Al and O as well. It is worth to notice that in this zone, a longitudinal crack occurred. Occurrence of such cracks may result in further spallation of almost entire oxidized layer. Such phenomenon probably occurred after oxidation at 900°C (Fig. 7).

Fig. 7a shows LM micrograph of Co-Ni-Al-W alloy oxidized at 900°C. The appearance of scale is in accordance with macrograph (Fig. 1). The substantial spallation of oxidation products occurred after experiment. SEM micrographs (Fig. 7a and Fig. 7b) show residual layers which did not peel after cooling to room temperature. The BSE image contrast imply that the upper part (marked by letter "C") may be enriched in W, which may be connected with $CoWO_4$ oxide. The discussed complex oxide was the dominant phase recognized after oxidation at 900°C via XRD. Moreover, the analogous area was observed around the crack in the scale of alloy oxidized at 800°C (Fig. 6c). Underneath, the other zone of internal oxidation (marked by letter "B") was noticed. This area is probably corresponding to internal oxidation zone after oxidation at 800°C ("B" in Fig. 6c).

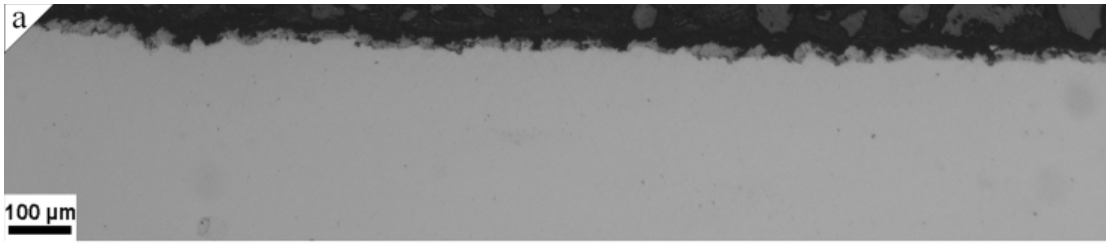

Optical micrograph

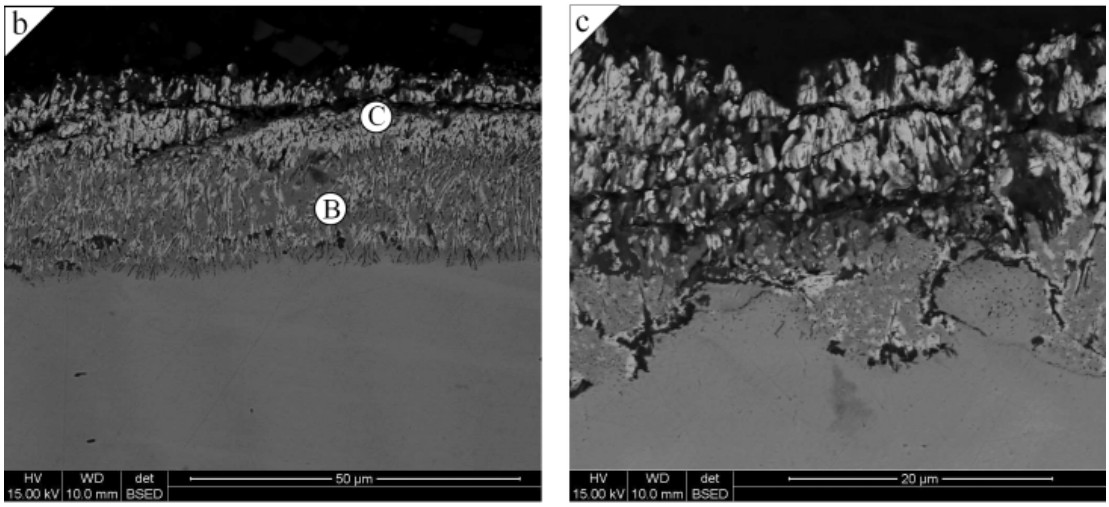

SEM micrographs

d Micro-area chemical composition in zones marked in SEM micrographs

Element/Area	Weight%					Atomic%				
	O	Al	Co	Ni	W	O	Al	Co	Ni	W
B	+	10.3	25.6	46.9	17.2	+	3.6	41.1	35.7	41.1
C	+	5.4	46.3	7.7	40.6	+	1.3	25.4	4.2	69.1

Fig. 7. Cross-sectional micrographs of the scale grown on Co-20Ni-7Al-7W alloy after oxidation at 900°C: a) LM micrograph; b and c) SEM micrographs; d) EDS analysis

In order to investigate a distribution of elements within the scale, the appropriate energy dispersive spectroscopy elemental mapping images were made (Fig. 8). The two-dimensional mapping images present qualitatively spatial distributions and local enrichments of the individual elements. The external layer ("A"), according to expectations, is mainly composed of O and Co. However, the discussed zone is also enriched in Ni, which implies formation of Ni oxides and their further dissolution resulting in formation of $(Co, Ni)_3O_4$ and (Co, Ni)O oxides. The inner oxide layer is composed of two sublayers, the upper one (around the crack) is considerably enriched in W ("C"). These areas are also rich in Al, however, depleted in Co and Ni. Underneath, the lower part of inner oxide layer is depleted in Co, and is rich in Al, W, and especially in Ni ("B"). In the case of alloy oxidized at 900°C, the dominant element in the upper part of the scale is W, which is related with the results of XRD (Fig. 3c). In this case, also underneath W-rich area, the substantial Ni-enrichment occurred.

The cross-sectional SEM images of the scale grown on Co-20Ni-10Al-5Mo-2Nb (at. %) alloy at 800 and 900°C may be seen in Fig. 9. In the case of both oxidation temperatures, a similar morphology of a residual oxide layer may be observed. The observable oxidation products are a mixture of different oxides based on Co, Nb, Mo and Al, which is more visible taking into account the distribution of elements (Fig. 10). In the case rof W-fee alloys, the accumulation of Ni underneath the oxide scale was observed as well. After oxidation at 800 and 900°C, the thickness of oxidized layer that remained after cooling to room temperature was very thin, therefore, X-ray diffraction (Fig. 4) revealed solid solution of cobalt.

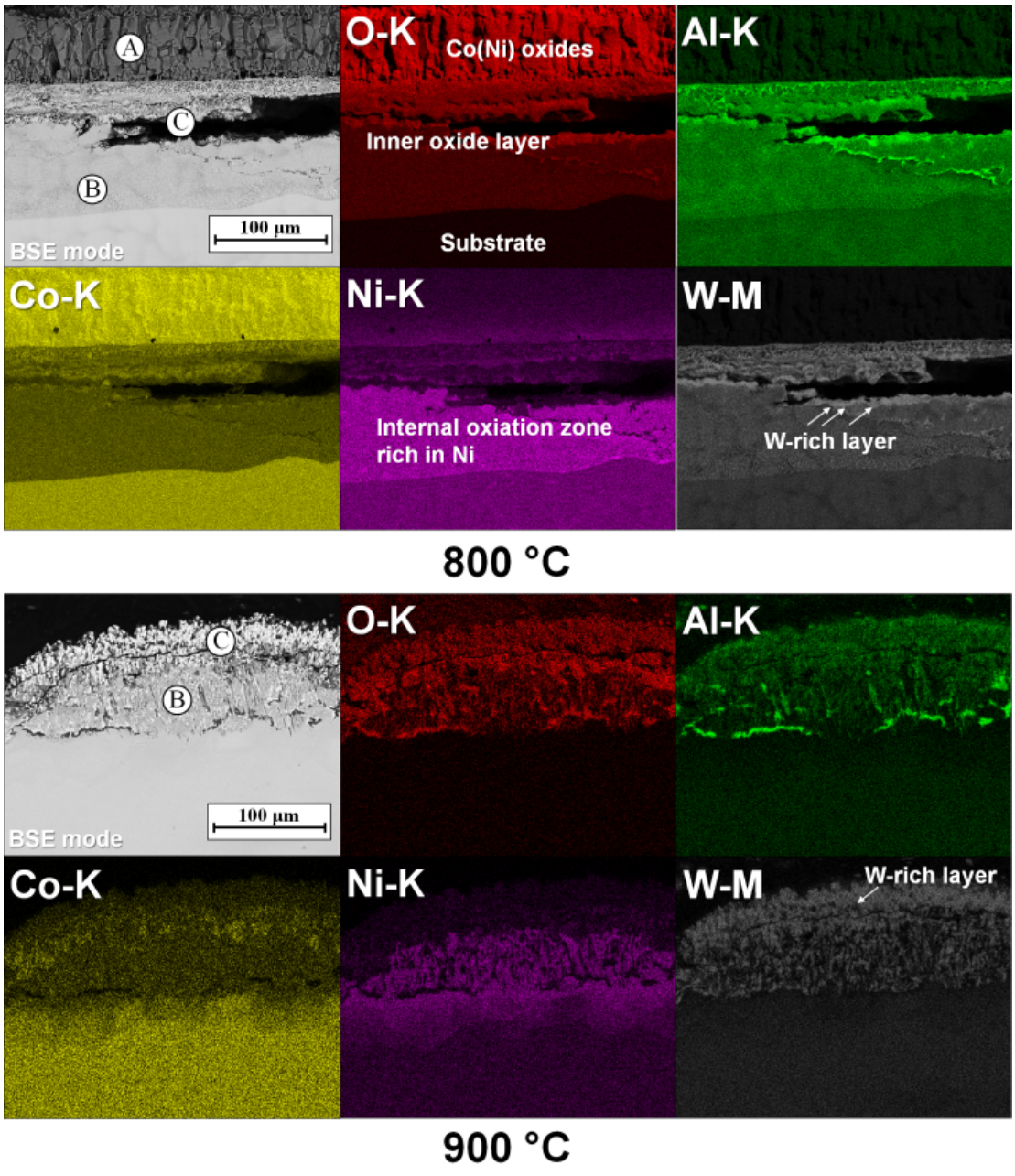

Fig. 8. Qualitative elemental mapping images of O, Co, Ni, Al, W in cross-section of scale grown on Co-20Ni-7Al-7W alloy after oxidation at 800°C and 900°C

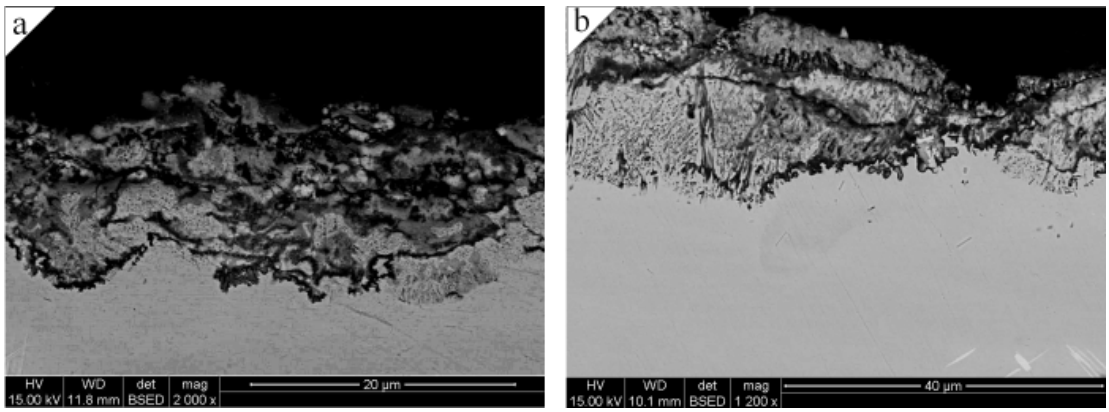

Fig. 9. Cross-sectional micrographs of the scale grown on Co-20Ni-10Al-5Mo-2Nb alloy after oxidation at: a) 800°C; b) 900°C

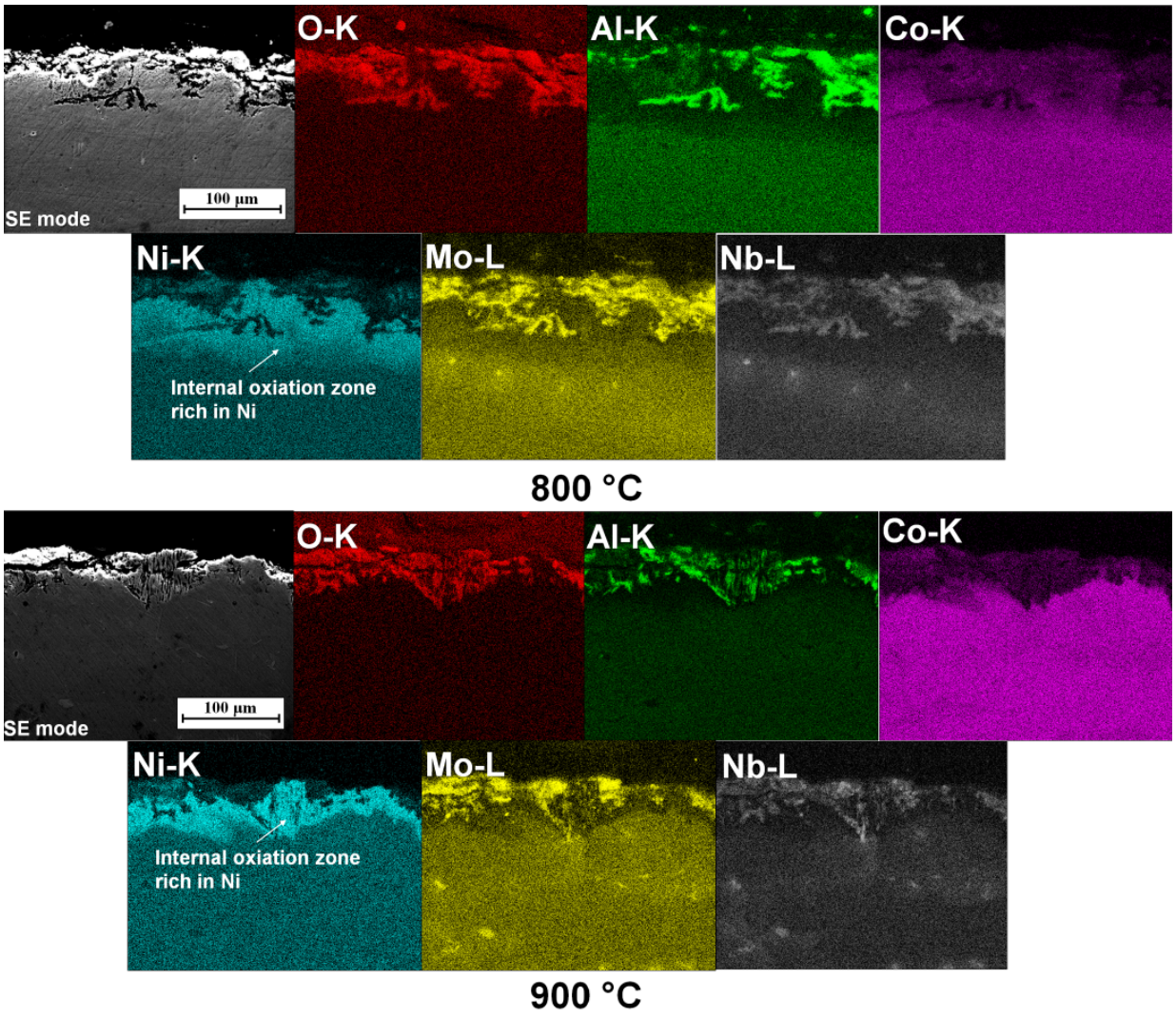

Fig. 10. Qualitative elemental mapping images of O, Co, Ni, Al, Mo, Nb in cross-section of scale grown on Co-20Ni-10Al-5Mo-2Nb alloy after oxidation at 800°C and 900°C

Fig. 11 shows the microstructure of scale grown after oxidation of Co-20Ni-7Al-7Ta (at. %) alloy at 800°C. A thickness of the oxidized layer was over 100 µm. The external, porous layer of Co(Ni)-oxides may be seen ("A"). Underneath, inner oxide layers are present (marked by "B" and "C"). In this zone, bright oxide particles with irregular morphology are observable. BSE image contrast implies enrichment in Ta. Within the substrate ("D"), typical γ–γ' region may be observed [20]. Moreover, numerous Co-Ta precipitates are also present in the substrate, which imply, such content of Ta is unfavourable in view of the microstructure. Taking into account the Co-Ta system [20], in this temperature range, γ, γ', χCo_7Ta_2 and C36 phases may be present.

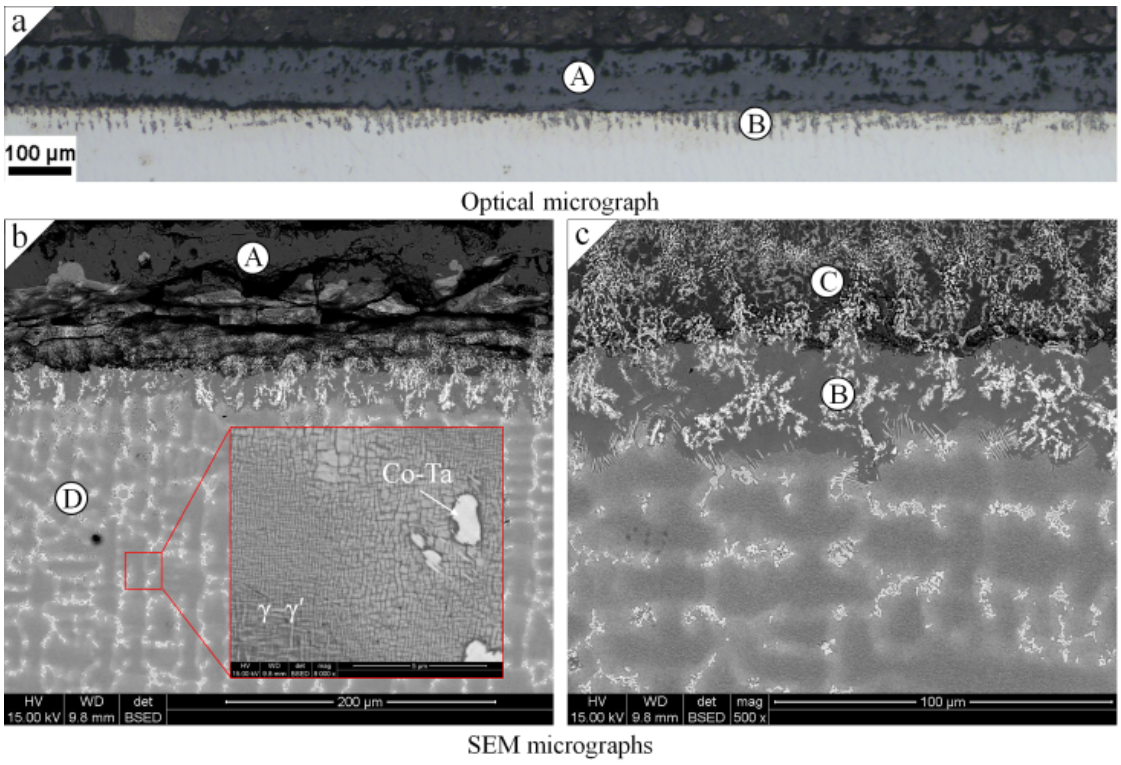

d Micro-area chemical composition in zones marked in SEM micrographs

Element/Zone	Atomic%					Weight%				
	O	Al	Co	Ni	Ta	O	Al	Co	Ni	Ta
A	+	-	100	-	-	+	-	100	-	-
B	+	9.3	46.2	32.6	11.8	+	3.6	38.8	27.2	30.4
C	+	10.6	26.2	20	43.2	+	2.6	14.2	10.9	72.3
D	-	6.9	66.8	19.6	6.7	-	2.9	60.5	17.7	18.9

Fig. 11. Cross-sectional micrographs of the scale grown on Co-20Ni-7Al-7Ta alloy after oxidation at 800°C: a) LM micrograph; b and c) SEM micrographs; d) EDS analysis

The microstructure of Co-20Ni-7Al-7Ta alloy after oxidation at 900°C is shown in Fig. 12. The inner oxide zone ("B") is corresponding to analogous zone, which occurred after oxidation at 800°C (Fig. 11c). The other zones spalled as a result of cooling to room temperature. The microstructure of the substrate alloy is analogous to that of after oxidation at lower temperature, however, except of Co-Ta phases present after oxidation at 800°C, numerous phases characterized by needle-like morphology may be observed. The morphology of observed phase constituent is similar to that of $D0_{19}$ phases occurring after high temperature oxidation of Co-Al-W alloys [7]. Fig. 13 shows distribution of elements in the scale of Co-20Ni-7Al-7Ta (at. %) alloy after oxidation at 800 and 900°C. The elemental mapping images imply that oxidation of alloy based on Co-Ni-Al-Ta system results in formation of the scale composed of 3 characteristic zones. The first one is zone of $Co(Ni)_3O_4$(upper part) and Co(Ni) (lower part) oxides ("A"). Underneath, inner oxide layer of oxidation products rich in Al and Ta is present ("C"). This layer was not observed after oxidation at 900°C due to spallation. The third layer is internal oxidation zone composed of Co_{ss} (substantially enriched in nickel) and a mixture of oxides with irregular morphology, enriched in Al and Ta ("B"). The X-ray diffraction analysis implied occurrence of $CoTa_2O_6$, Ta_2O_5 and Al_2O_3 oxides (Fig. 5b). Below the oxidized zones, substrate alloy characterized by γ–γ' microstructure and numerous Co-Ta eutectic precipitates may be seen. The enrichment of internal oxidation zone by Ni was observed for all Co-Ni alloys. It could be attributed to rapid depletion of substrate alloy in Co, whereas Ni had lower affinity for oxygen that is in accordance with free energy of oxides formation [21]. The considerations concerning the internal structure of the scale can ban be based on CALPHAD modeling [19,22]. The computational results show that the scale grown of Co-Al-W superalloys is composed of MO oxides (halite type of lattice), M_3O_4 oxides (spinels), MO_2 oxides (rutile type of lattice) and tungstates (e.g. $CoWO_4$). The transition and inner zones cover the internal oxidation area and contain, respectively, a γ' free zone and spinels with a small amount of oxides with a rutile type of lattice and, a γ/γ' matrix with corundum phases (alumina, chromia). The theoretical predictions are in accordance with experimental results. The similar scale formation may concern Co-20Ni-7Al-7W/7Ta (at. %) alloys. In the case of Co-20Ni-10Al-5Mo-2Nb, the scale structure was quite similar to that of Co-10Al-5Mo-2Nb (at. %) alloy [15].

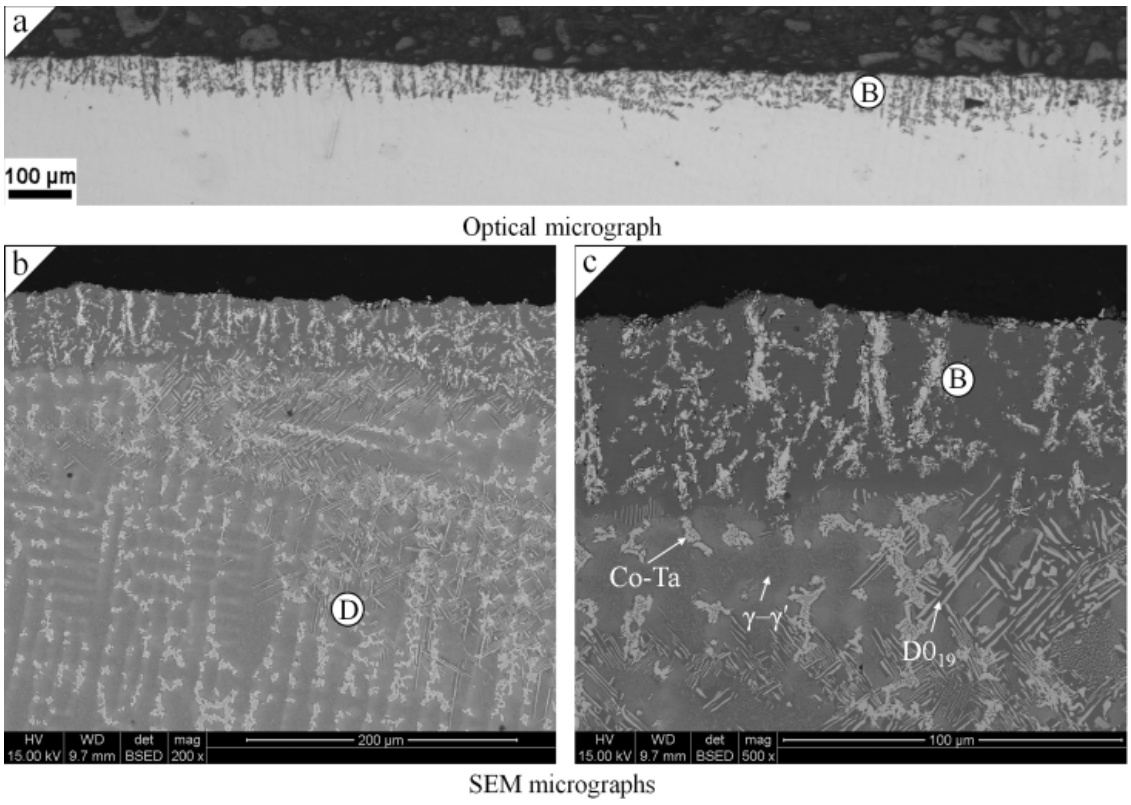

d Micro-area chemical composition in zones marked in SEM micrographs

Element/Zone	Atomic%					Weight%				
	O	Al	Co	Ni	Ta	O	Al	Co	Ni	Ta
B	+	9.3	48.6	29.3	12.8	+	3.5	40.1	24.1	32.3
D	-	7.2	66.5	19.5	6.8	-	60.3	17.6	2.9	19.2

Fig. 12. Cross-sectional micrographs of the scale grown on Co-20Ni-7Al-7Ta alloy after oxidation at 900°C: a) LM micrograph; b and c) SEM micrographs; d) EDS analysis

4. Summary

The thermogravimetric analysis as well as isothermal oxidation test showed that Co-Ni based alloys containing such alloying elements as Al and W; Al, Mo and Nb; Al and Ta, exhibit low oxidation resistance. The oxidation rate in these cases was relatively high, moreover, after cooling to room temperature from 900°C, the effect of substantial spallation of oxide layer occurred. This effect was the most intensive in the alloy with Mo and Nb. In this case, considerable peeling of oxides occurred even for oxidation at 800°C. For other alloys oxidized at 800°C, the oxide scale was characterized by occurrence of external porous layer of Co(Ni) oxides, inner oxide layer composed of mixed oxides of Co, Al, W, Ta, and, the internal oxidation zone substantially enriched in nickel. The scales grown on alloys at 900°C were characterized by inner oxide zones characterized by complex phase composition, including mixed oxides such as $CoWO_4$, $CoTa_2O_6$, $Co_2Mo_3O_8$ and $CoNb_2O_6$. Occurrence of such phases may result in further spallation of oxide scales, which was especially visible in the case of Co-20Ni-7Al-7W after oxidation at 800°C. In this case, considerable cracks were observed in areas rich in W, which could contain substantial amount of $CoWO_4$.

Acknowledgments

This work was supported by National Science Centre (Project 2018/29/N/ST8/02062).

Publication was supported by the Rector's Grant in the field of research and development, Silesian University of Technology, Grant Number 11/030/RGJ19/0234.

REFERENCES

[1] J. Sato T. Omori, K. Oikawa, I. Ohnuma, R. Kainuma, K. Ishida, Sci. **312**, 90-91 (2006).

[2] Y. Chen, C. WAng, J. RUan, T. Omori, R. Kainuma, K. Ishida, X. Liu, Acta Mater. **170**, 62-74 (2019).

[3] S.K. Makineni, B. Nithin, K. Chattopadhyay, Scr. Mater. 98, 36-39 (2015).

[4] F.L. Reyes Tirado, S. Taylor, D.C. Dunand, Acta Mater. **172**, 44-54 (2019).

[5] J.J. Ruan, J. Liu, S.Y. Yang, W.W. Xu, T. Omori, T. Yang, B. Deng, H.X. Jiang, C.P. Wang, R. Kainuma, K. Ishida, Intermetallics. **92**, 126-132 (2018).

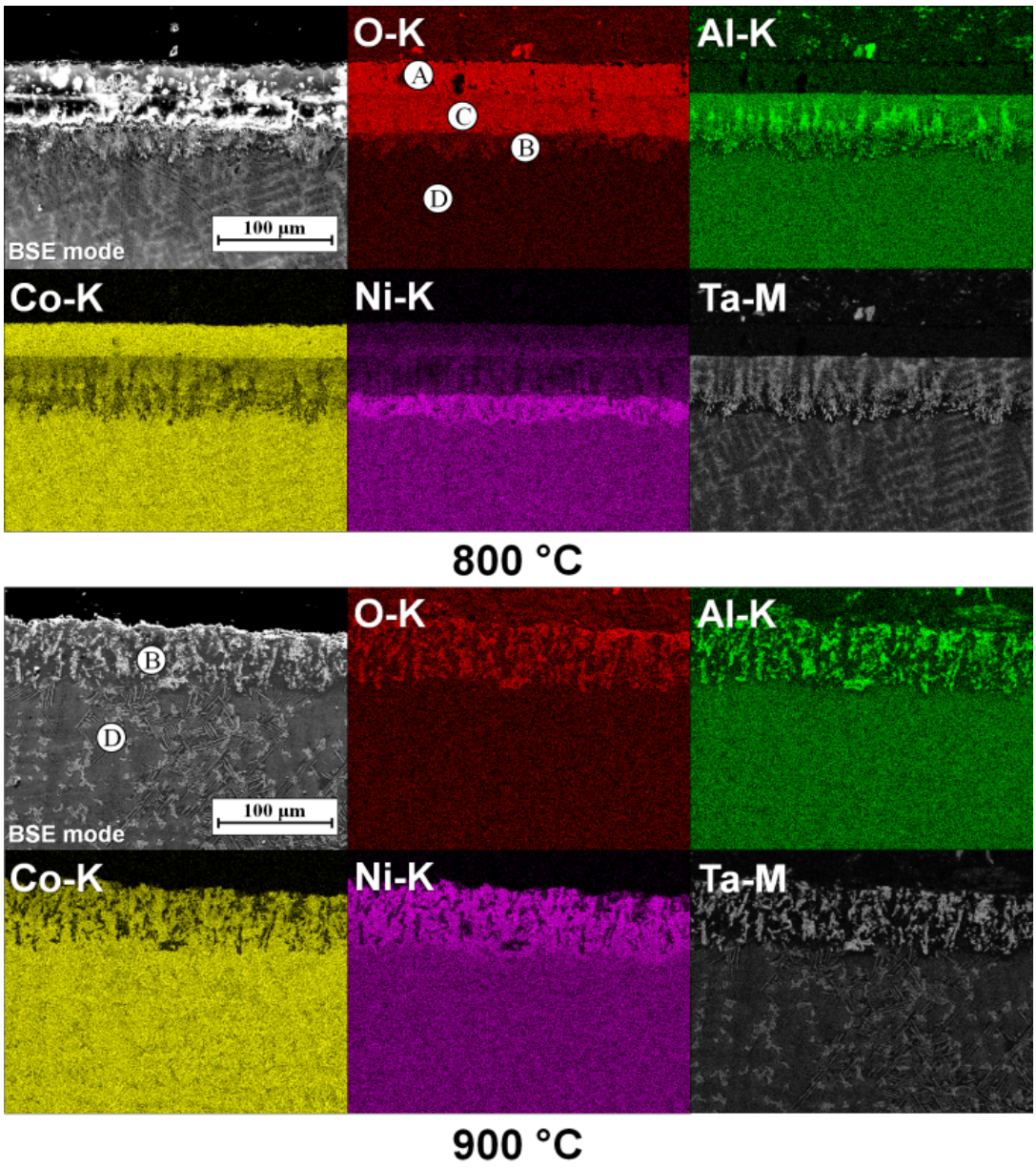

Fig. 13. Qualitative elemental mapping images of O, Co, Ni, Al, Ta in cross-section of scale grown on Co-20Ni-7Al-7Ta alloy after oxidation at 800°C and 900°C

[6] H.-Y. Yan, V.A. Vorontsov, D. Dye, Intermetallics. **49**, 44-53 (2014).

[7] L. Klein, A. Bauer, S. Neumeier, M. Göken, S. Virtanen Corros. Sci. **53**, 2027-2034 (2011).

[8] H.-Y. Yan, V.A. Vorontsov, D. Dye, Corros. Sci. **83**, 382-395 (2014).

[9] M. Weiser, Y.M. Eggeler, E. SPiecker, S. Virtanen, Corros. Sci. **135**, 78-86 (2018).

[10] M. Weiser, S. Virtanen, Oxid. Met. **92**, 541-560 (2019).

[11] C.A. Stewart, A. Suzuki, R.K. Rhein, T.M. Polock, C.G. Levi, Metall. Mater. Trans. **50**, 5445-5458 (2019).

[12] M. Weiser, M.C. Galetz, H.-E. Zschau, C.H. Zenk, S. Neumeier, M. Göken, S. Virtanen, Corros. Sci. **156**, 84-95 (2019).

[13] B. Gao, L. Wang, Y. Liu, X. Song, S.Y. Yang, A. Chiba, Corros. Sci. **157**, 109-115 (2019).

[14] S.M. Das, M.P. Singh, K. Chattopadhyay, Corros. Sci. **155**, 46-54 (2019).

[15] D. Migas, G. Moskal, D. Niemiec, J. Mater. Eng. **27**, 447-456 (2018).

[16] D. Migas, G. Moskal, M. Mikuskiewicz, T. Maciąg, J. Therm. Anal. Calorim. **134**, 119-125 (2018).

[17] A. Tomaszewska, G. Moskal, T. Mikuszewski, G. Junak, A. Płachta, Arch. Foundry Eng. **19**, 78-73 (2019).

[18] D. Migas, G. Moskal, T. Maciąg, Thermal analysis of W-free Co-(Ni)-Al-Mo-Nb superalloys, Journal of Thermal Analysis and Calorimetry, in press (DOI: 10.1007/s10973-020-09375-7)

[19] S.A. Forsik, A.I. Polar Rosas, G.A. Colombo, N. Zhou, S.J. Kenion, M.E. Epler, Metall. Mater. Trans. **49**, 4058-4069 (2018).

[20] K. Shinagawa, H. Chinen, T. Omori, K. Oikawa, I. Ohnuma, K. Ishida, R. Kainuma, Intermetallics. **49**, 87-97 (2014).

[21] H.J.T. Ellingham, J. Soc. Chem. Ind. **63**, 125-133 (1944).

[22] L. Klein, A. Zendegani, M. Palumbo, S.G. Fries, S. Virtanen, Corros. Sci. **89**, 1-5 (2014).